25TH INTERNATIONAL CONGRESS OF THE AERONAUTICAL SCIENCES

Sonic Boom Prediction, Focusing and Mitigation

O. A. Kandil [1], I. A. Ozcer [2], Nitin Khasdeo[3]
Aerospace Engineering Department
Old Dominion University, Norfolk, VA 23529, USA

Abstract

Supersonic travel over land would be a reality, if new aircraft are designed such that they produce quieter ground sonic booms, no louder than 0.3 psf according to FAA requirement. To accomplish this challenging goal, research has to be focused on three phases of research work, which are addressed in this paper. The first phase is focused on development of advanced prediction tools for shock waves emanating from aircraft and propagating to the ground, 6-8 miles away from the aircraft. This phase is completed and two applications are demonstrated, which cover the F-5E aircraft and a double cone configuration. The second phase is focused on development of prediction tools for sonic boom focusing (superboom), which develops during aircraft accelerations during climbing, turning and maneuvering. Several schemes, which use the numerical solution of the nonlinear Tricomi equation, have been developed and their results are demonstrated through several computational applications. The third phase is focused on the development of mitigation techniques of sonic boom strength to reduce the ground boom signature. A few applications; which use the wing dihedral angle and addition of a boom piece to the aircraft nose, are presented.

1. Introduction

In this paper, we address each of these three areas of research work; prediction, focusing and mitigation, and present current computational applications and current and future progress as well. In the following sections, each area of research work is presented and the results are discussed.

1. Professor and Eminent Scholar, Assoc. Fellow AIAA
2, 3 PhD Graduate Research Assistant, Member AIAA

2. Sonic Boom Prediction

2.1 Background

For sonic boom computation and prediction, the near-field domain around the aircraft is computed using an Euler-equations solver which is a modified CFL3D code. In the far-field domain the full-potential equation is numerically solved. The reason behind choosing the full-potential equation versus using the Euler equations or the multi-pole linear equation for the far-field computations is computational efficiency (versus the substantial computational time needed for the Euler equations marching several miles [6-8 miles]), and carrying the nonlinear effects of the propagating waves (versus the multi-pole linear equation). At the interface plane between the Euler near-field solution and the full-potential solution, velocity components of the Euler-equations solver are transformed into a velocity potential that is used as the initial condition of the full potential solver. Starting with this interface solution, the conservative form of the steady full-potential equation is used with a space-marching, upwind scheme [1], [3-4]. This scheme is "augmented" by a main block/sub-block technique which accommodates the treatment of the varying speed of sound with altitude. Grid adaptation and physical-geometrical shock fitting (SFGA) schemes have been developed and applied to the Euler equations near-field solver and the main blocks and sub-blocks of the far-field full-potential equation solver.

2.2 Computational Applications

The capability of the newly-developed full-potential propagation code is demonstrated for predicting the sonic-boom ground signature of the

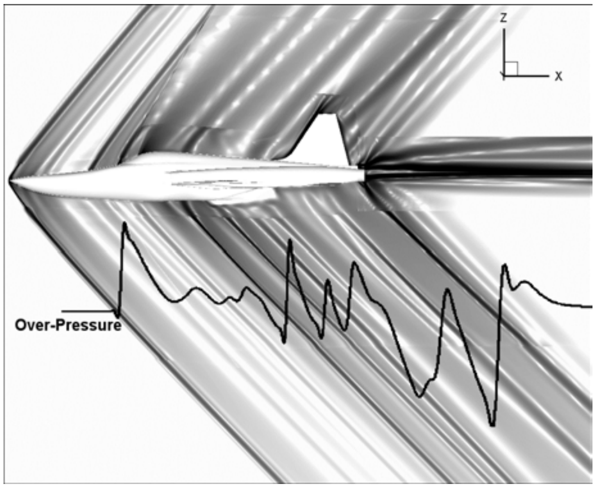

Fig. 1: Schlieren photo of the near-field solution of the F5-E modified aircraft

modified F-5E aircraft used in the F-5 "Shaped Sonic Boom Experiment" (SSBE) Program. The computational application is that of a modified F-5E flight 15, which was conducted by Northrop-Grumman Company on January 13, 2004. Figure 1 shows the Schlieren density contours at h/L = 1.82 (91ft) below the aircraft, which are computed by the modified CFL3D Euler code using the Northrop-Grumman structured grid (23 multi-blocks with a total of 17 mil grid points) and flow conditions. Here, the modified F-5E aircraft is at a 32,686ft altitude, 1.92^{o} angle of attack and 1.414 Mach number. Figure 2 shows a good comparison of the computed ground overpressure using the present full-potential (FP) code with the measured field data provided by Northrop- Grumman.

Next, the structured-grid CFL3D code is modified and applied to a double-cone configuration, Ref. [5](see Fig. 3). The flow Mach numbers are 1.26 and 1.41 and the angle of attack is zero. The CFL3D code is modified using a new, highly accurate grid-adaptation and physical and geometrical shock-fitting (SFGA) schemes for supersonic near-field domain prediction. Physical shock fitting is accomplished using the gradient of density and Mach on the coordinate lines crossing the shock. One of these coordinate lines is designated to be ξ^2.Gradient of density is evaluated as $|\nabla\rho|$ whereas gradient of Mach is evaluated as

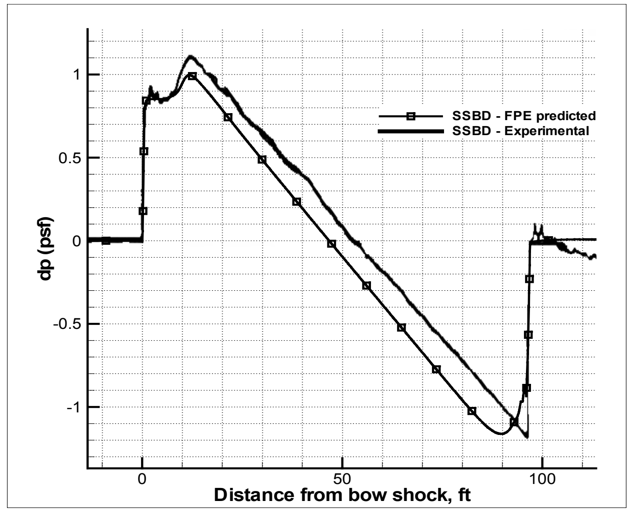

Fig. 2: Comparison of the FP predicted results with the measured SSBE ground overpressure for the modified F-5E at ground (h = 2.372ft)

the derivative of Mach with respect to ξ^2 ,$\partial M/\partial\xi^2$. Both of these gradients peak at the shocks, and stay mostly leveled in the remaining regions. Thus, they form sets of data that can be used to locate shocks in the solution. Theoretically, this data should be a smooth curve with peaks occurring only at shocks. Since the idea is to eventually obtain each shock on a single grid line, Rankine-Hugoniot (R H) equations are to be used across a single grid line. Depending on the magnitude of the errors in mass, momentum and energy, one can cease to continue with the next iteration. If the errors are large enough, a grid generation process for the captured shock points begins. The captured shock points are fitted with 5^{th} order polynomials to come up with an algebraic equation that can be used in the grid generation process. The polynomial coefficients are input to the grid generation scheme and the grid is generated. The polynomials for the shocks are used to create foundation gridlines for the grid block. Grid adaptation is also based on the density gradients. This scheme is called new shock-fitting grid adaptation (SFGA) scheme. This scheme is also used with the far-field full-potential equation solver.

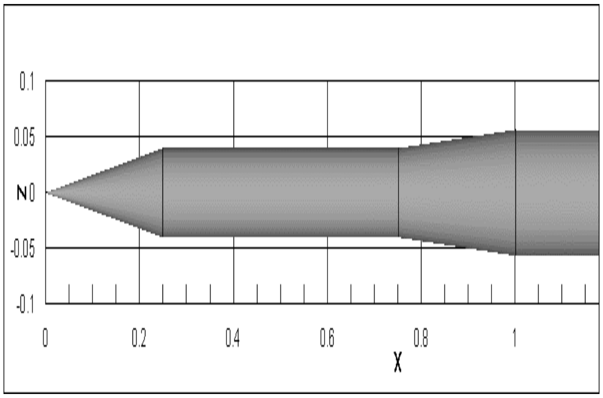

Fig. 3: Side-view of the dimensionless double-cone configuration (Ref. 5).

Figs. 4 and 5, show the converged results of the modified CFL3D near-field solver for the sequence of SF2-GA1-SF1-GA1-SF5, where SF stands for shock fitting and GA stands for grid adaptation. The new SFGA scheme is obviously producing sharper accurate shocks without over shootings or under shootings at the captured-fitted shocks.

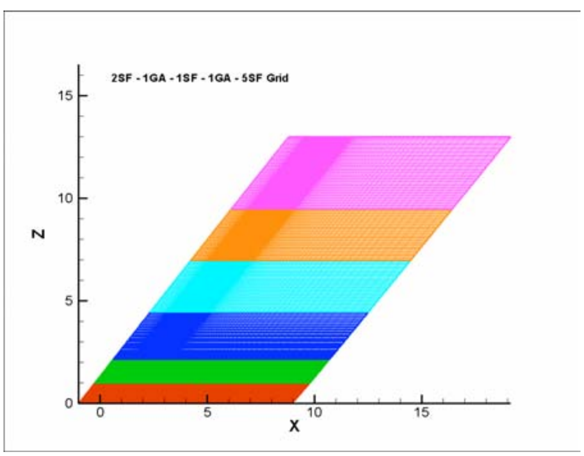

Figure 4: Converged grid after SF2-GA1-SF1-GA1-SF5 for a double cone, M = 1.26.

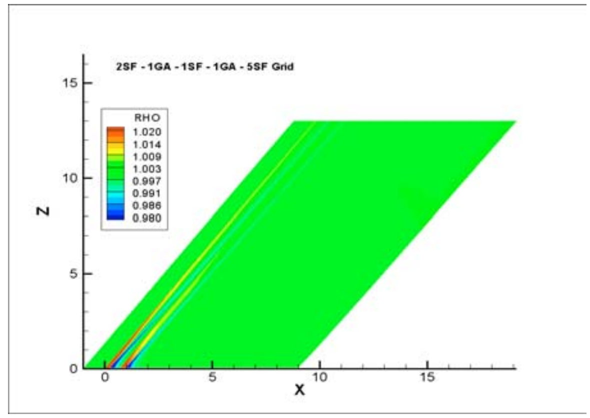

Fig. 5: Density contours after SF2-GA1-SF1-GA1-SF5 for a double cone M = 1.26.

Unstructured grid technology promises easier initial grid generation for novel complex three-dimensional (3D) configurations as compared to the structured grid techniques. The use of unstructured grid technology for CFD simulations allows more freedom in adapting the discretization of the meshes to improve the fidelity of the simulation. Many previous efforts attempted to tailor the discretizations of unstructured meshes to increase solution accuracy while reducing computational cost, Ref. [6]. The FUN3D Code accuracy has been evaluated for the near-field computations for capturing shocks and adapting the unstructured grid. The adjoint variable approach (solution of the dual problem) is an efficient method for computing derivatives of a function of interest for gradient-based design methods. Some examples of discrete adjoint design methods are given in Anderson[7] and Nielsen[8].

In the present paper, the unstructured FUN3D near-field code is applied to the double-cone configuration at a Mach number of 1.26. The CFL3D code is modified by using the new SFGA scheme and is applied also to the same double-cone configuration with Mach number of 1.26. The results of the two codes are compared with the experimental data of Ref. [5]. Next, an interface-plane interpolation scheme has been developed between the FUN3D code and the efficient FP Far-field code at an altitude to configuration length of h/L= 2. The interpolation errors have been computed. The same matching is done with the modified CFL3D. Next, the FP code is modified using the new SFGA scheme, and used to propagate the interface results to h/L = 6, 10, 18 and very high far-field locations as well. The results of the FUN3D-FP coupled code and the modified CFL3D-FP coupled code are compared with the experimental data.

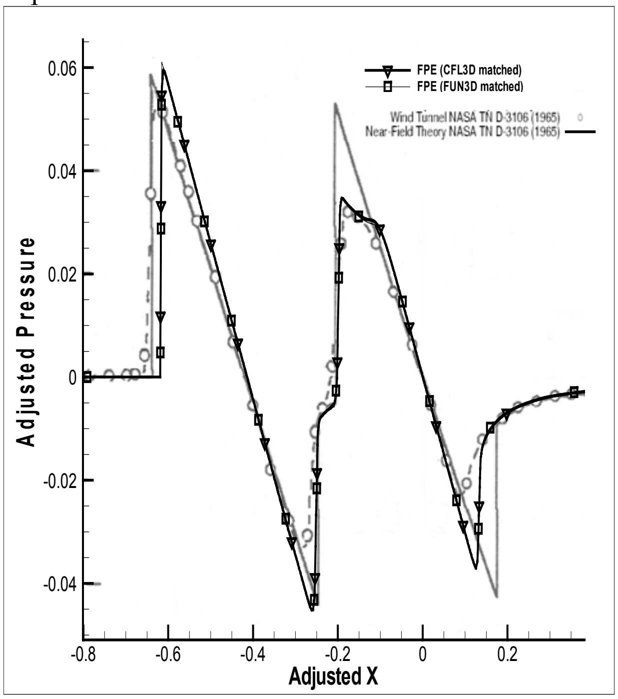

Fig. 6: Adjusted pressure signatures at *h/L =10*, comparing both FP matched solutions with FUN3D and CFL3D with the experimental data.

The FP matched interface solutions obtained from FUN3D and CFL3d are marched to h/L = 6 and then to h/L =10, 18, 40 and 70. Figure 6 shows a comparison of the adjusted pressure versus the adjusted x distance at h/L = 10 of the FP matched with FUN3D and the FP matched with CFL3D. The comparison shows excellent agreement. These results are compared with the experimental data in Fig.6, which again shows excellent agreement. Figure 7 shows similar comparisons as those of the previous case but at h/L = 18. It is conclusively clear that the FP matching with FUN3D is highly accurate and efficient.

3. Sonic Boom Focusing

3.1 Background

The most intense sonic boom is the focused sonic boom due to aircraft transonic acceleration from Mach 1 to cruise speed. Sonic boom focusing develops also due to aircraft turns and maneuverings. It leads to amplification of ground pressures up to two or three times the carpet boom shock strength. Therefore, accurate prediction of focused sonic booms at the caustic near ground

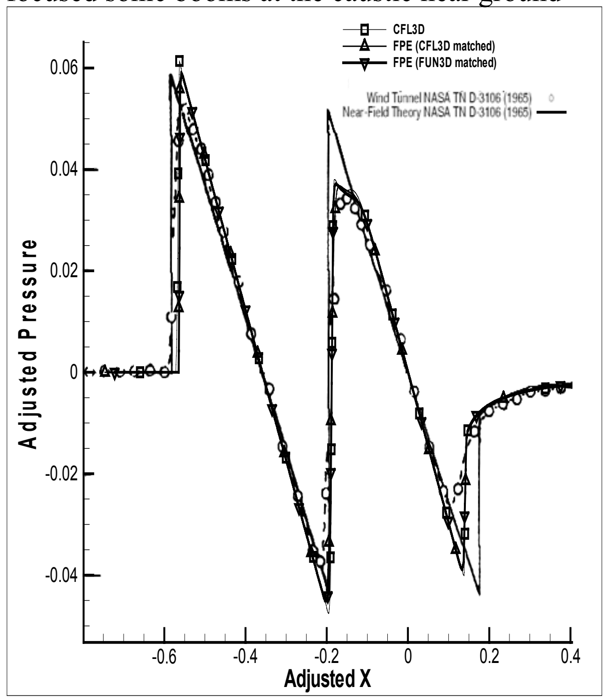

Fig. 7: Adjusted pressure signatures at *h/L =18*, comparing both FP matched solutions with FUN3D and CFL3D with the experimental data and CFL3D marching.

level is very important. Sonic boom focusing has been also known as “sonic superboom”.

Focusing of shock waves occurs at surfaces called caustics. Caustics are regions of wave amplification and geometrical ones. Shock wave focusing is fundamentally a nonlinear process. Here the emphasis is directed to the smooth caustic surface case. Analysis of weak shock focusing at a smooth caustic surface has been introduced in 1965 by Guiraud [9]. He developed a theory, which includes both diffraction and nonlinear effects up to first order, which leads to the nonlinear Tricomi equation. This result was confirmed by Hayes [10], Hunter and Keller [11], and Rosales and Tabak [12], [13]. Augar and Coulouvrat [14] have presented a FD algorithm to solve the nonlinear Tricomi equation, which was expressed in terms of the dimensionless acoustic pressure. Recently, Marchiano and Coulouvrat [15] have solved the nonlinear Tricomi equation in terms of the potential field instead of the pressure field using the FD scheme. The nonlinear effects were treated using an "exact" solver. Kandil and Zheng [16], [17] have solved the nonlinear non-conservative Tricomi equation using the frequency-domain scheme (FFT), a time-domain (TD) scheme and a TD with overlapping grid (OLG) scheme. A conservative form of the nonlinear Tricomi equation has been developed and solved using a time-domain scheme (CTD). The four schemes have been applied to several incoming waves which include an N wave, a Concorde aircraft wave and symmetric and asymmetric flat-top and ramp-top waves.

In Ref. [18] a parametric study has been carried out to investigate the effects of several parameters on the sonic-boom focusing computational results obtained from the nonlinear Tricomi equation. The CTD scheme is used in this study.

3.2 Computational Applications

The steady nonlinear Tricomi equation is modified [15] as an unsteady equation by adding a pseudo unsteady term $\partial^2 \phi / \partial \tau \partial t$, which will tend to zero when the pseudo time marching scheme reaches the steady solution of $\phi(t \to \infty, \tau, z)$. The modified equation is given by

$$\frac{\partial^2 \phi}{\partial \tau \partial t} = \frac{\partial^2 \phi}{\partial z^2} - z \frac{\partial^2 \phi}{\partial^2 \tau} + \frac{\mu}{2} \frac{\partial}{\partial \tau} \left[\left(\frac{\partial \phi}{\partial \tau}\right)^2 \right] \qquad (1)$$

Where

ϕ = acoustical potential

t = pseudo time variable

τ = dimensionless phase variable = [t – x (1-z / R_{sec}) / c_0] / T_{ac}

The boundary conditions [15] to be satisfied are:

1. no disturbance before or after acoustic waved has passed

$$\phi(z, \tau \to \pm\infty) = 0 \qquad (2)$$

or for a periodic signal with period T

$$\phi(z, \tau + T) = \phi(z, \tau)$$

2. away from the caustic surface in the shadow zone the acoustic pressure decreases exponentially:

$$\phi(z \to -\infty, \tau) \to 0 \qquad (3)$$

3. a radiation condition is imposed (away from the caustic on the illuminated side the field matches the geometrical acoustic approximation)

$$z^{1/4} \frac{\partial \phi}{\partial \tau} + z^{-1/4} \frac{\partial \phi}{\partial z} \to 2F\left(\tau + \frac{2}{3} z^{3/2}\right) \qquad (4)$$

The unsteady nonlinear equation is split into two simpler equations. The first one includes the linear diffraction effects and the second one includes the nonlinear effects. Thus, the equation is split into the following two equations

$$\frac{\partial^2 \phi}{\partial \tau \partial t} = \frac{\partial^2 \phi}{\partial z^2} - z \frac{\partial^2 \phi}{\partial^2 \tau} \qquad (5)$$

and

$$\frac{\partial \phi}{\partial t} = \frac{\mu}{2} \left(\frac{\partial \phi}{\partial \tau}\right)^2 \qquad (6)$$

. Equation (5) can be solved in time-domain integration or in frequency-domain integration. Equation (6) can be solved using a shock-capturing finite-differencing scheme or by an exact shock fitting scheme.

We choose a rectangular domain with the ordinate $z \in [-2.0, 2.0]$ and the abscissa $\tau \in [-2.67, 3.67]$ dimensionless units. The number of grid points in the z direction is 1000. In the τ direction the number of grid points is 8,192 points when using the TD scheme, or 1, 024 frequencies when using the FD scheme. It should be noticed that the higher the grid points or the frequencies in τ direction are, the better the solutions are.

On the upper boundary z = 2.0 the incoming N-wave extends from τ = -1.386 to τ = – 2.386 (duration of 1) with p_{max} = 1.0 and p_{min} = -1 (τ & p are dimensionless). With these dimensionless pressure and duration, p = 1 is equivalent to 2.25 psf and τ = 1 is equivalent to 230 ms. The dimensionless time step for the pseudo time integration is taken as 0.001. The case has been run for 20,000 time steps until total error of the pseudo unsteady time term was reduced to 10^{-6}.Figure 8 shows the pressure contours of the incoming wave as it progresses in the domain toward the caustic surface, which is shown on the figure, and the outgoing wave as it originates from the caustic surface. This solution is obtained using the Frequency Domain scheme. In Fig. 9, it is noticed that the predicted wave at the caustic surface shows pressure peaks of 3.1, 1.54 and -1.7 (equivalent to 6.98psf, 3.47 psf and – 3.83 psf, respectively). These results conclusively show that the superboom response is predicted. It is also consistent with the results of Ref. [15]. Figures 10 and 11 show the interaction of the incoming wave with the outgoing wave at z = 2.0 and 0. Figures 12-14 show the corresponding results using the CTD Scheme. The conservative time domain (CTD) Scheme has been applied to the solution of the N-wave case. The computational domain and grid of the FD-Scheme have been used for this solution case. Figures 12-15 show the CTD results of this case. The captured caustic line is shown in Fig. 12. It is in excellent agreement with that of the FD Scheme. The p_{max} of Fig. 13 is 3.04 or 6.84psf, which is in excellent agreement with the previous result of FD solution. The solutions at z = 2.0, and 0 are in good agreement with the FD Scheme.

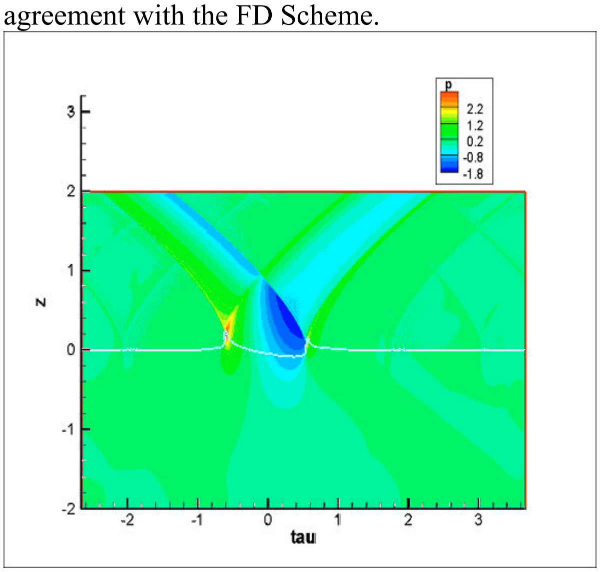

Fig. 8: Pressure contours for an incoming N-wave at nt = 20,000 time steps, FD solution.

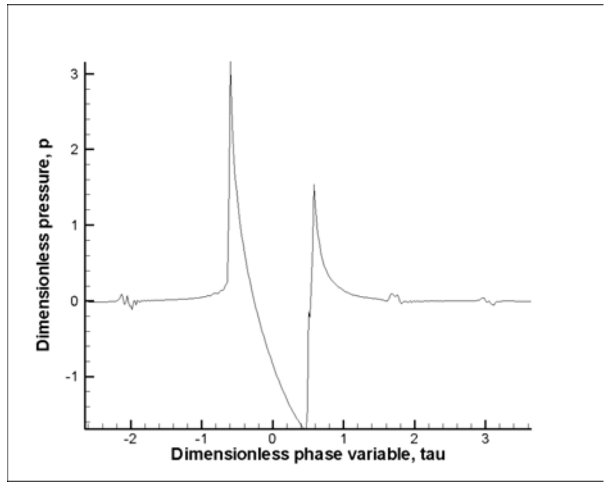

Fig. 9: Pressure variation for N-wave at z of p_{max} = 0.19 and nt = 20,000 steps, FD solution.

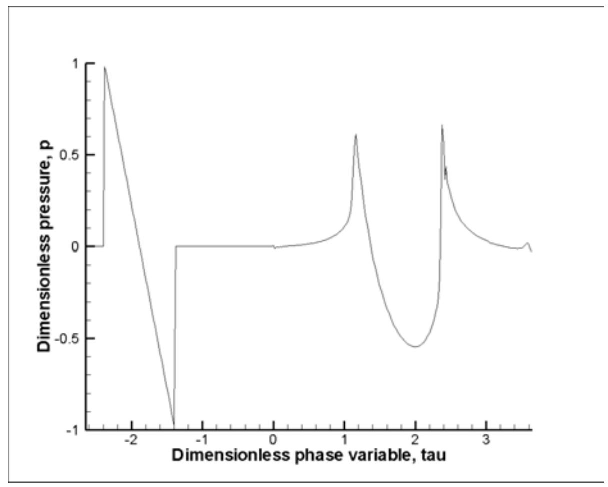

Fig. 10: Pressure variation for N-wave at z = 2.0 and nt = 20,000 steps, FD solution.

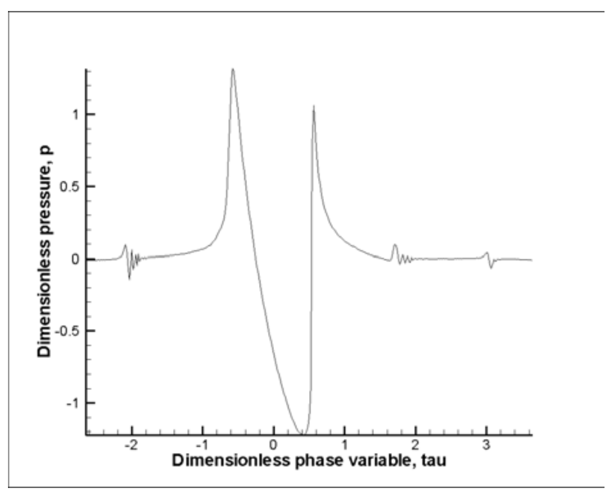

Fig. 11: Pressure variation for N-wave at z = 0 and nt = 20,000 steps, FD solution.

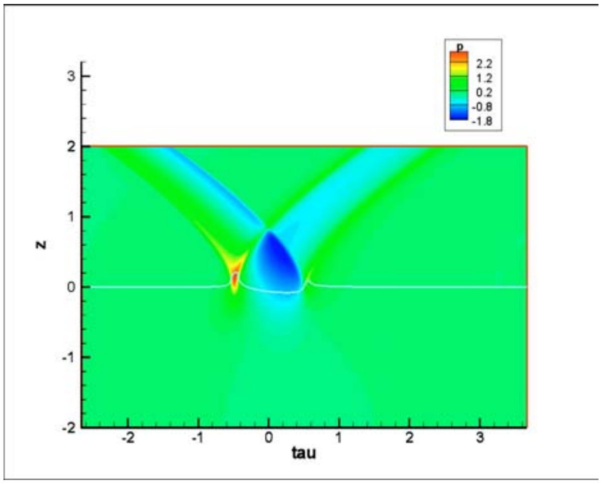

Fig. 12: Pressure contours for an N-wave at nt = 20,000 steps, CTD solution.

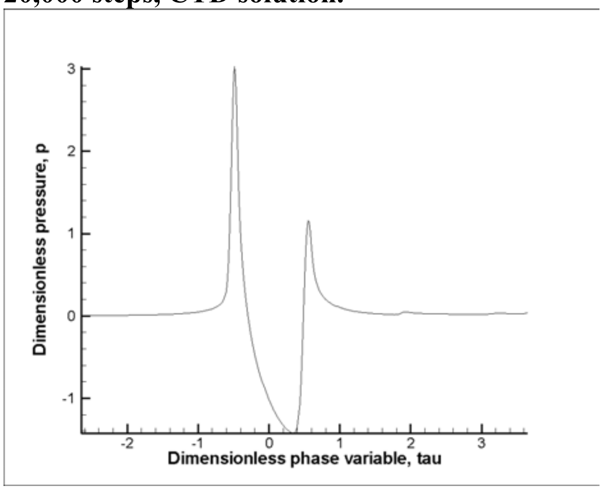

Fig. 13: Pressure variation for an N-wave at z of p_{max} = 0.14 and nt = 20,000 steps, CTD solution.

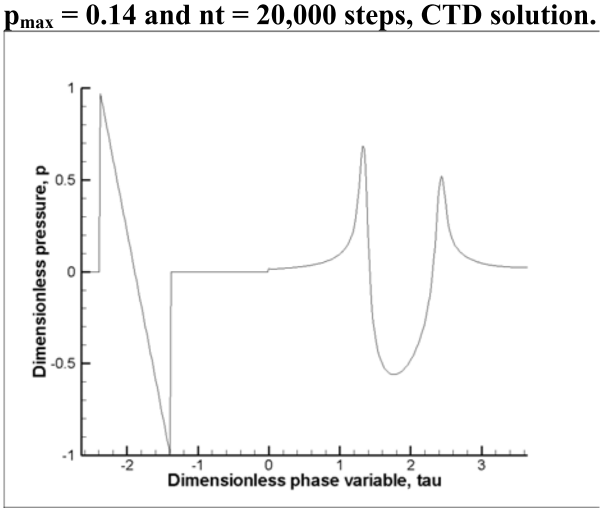

Fig. 14: Pressure variation for N-wave at z = 2.0 and nt = 20,000 steps, CTD solution.

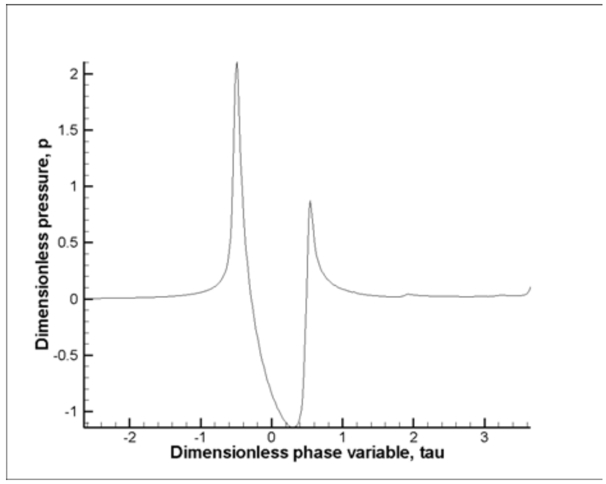

Fig. 15: Pressure variation for N-wave at z = 0 and nt = 20,000 steps, CTD solution.

4. Sonic Boom Mitigation

4.1 Background

Sonic boom noise has been an environmental concern almost as long as aircraft capable of supersonic flight have existed. These "booms" are the result of shock waves, or abrupt pressure increases, generated in the flow field of an aircraft flying at supersonic speeds, being propagated to the ground.

For most aircraft this signature has the shape of a capital "N" and consequently is called an N-wave. The initial rise in pressure, or shock, is due to the coalescence of various shock waves emanating from the forward components of the aircraft, while the aft pressure rise usually stems from shocks (including recompression shocks) emanating from the aft regions of the aircraft. Research aimed at reducing sonic boom attempts to reduce the magnitude of both the forward and aft pressure "jumps." In this endeavor the shape of the pressure wave is modified through the use of optimum longitudinal area distributions of the aircraft, including the effective area distribution due to lift [18]-[32]. Shapes (pressure signatures) that have been studied include a flattop, ramp, and a combination of the ramp and flattop called a hybrid (see Fig. 1) [23],[29]-[30]. A further variation of the flattop which might be called a "spiked" flattop ha also been studied and shown to have certain advantages [27], [28]. Clearly, the goal in supersonic configuration design, biased toward sonic boom minimization, should be to distribute lift and volume in such a way that the longitudinal and spanwise distribution of pressure propagated to the ground have the lowest possible pressure increments due to shocks, thus, minimizing the boom and associated physical discomfort and structural damage. One goal in striving to achieve this is a spanwise distribution of shock strengths (pressure jumps), on the ground, that is near uniform rather than the "normal" one, which has a pronounced maximum at the symmetry plane. In order to obtain a more uniform spanwise distribution it would seem that one must control, in an optimal way, the spanwise distribution of sweep, lift and volume. Dihedral has also been shown to have a significant beneficial effect on sonic boom [25], [33]. There are limits, however, in what can be achieved in making the spanwise distribution more uniform without increasing the overall boom level (if sweep is reduced) or aerodynamic drag (performance).

4.2 Computational Applications

One of the mitigation schemes that has been recently tried is to investigate the effects of adding a boom piece at a wing vertex on the ground over-pressure of the sonic boom wave. The study starts with a 5% maximum thickness, bi-convex delta wing at 2.24 angle of attack, 50,000 ft altitude and Mach number of 2.0. The problem is solved without a vertex boom addition using the CFL3D solver for the near-field domain and the Full-Potential equation solver for the far-field domain. Next, a boom with a diamond section is added at the vertex of the delta wing with a length of 0.1 of vertex shock wave and more than 30% of the trailing-edge shock wave. the wing root chord. The preliminary results of this case show more then 10% reduction of the wing-

A bi-convex (chordwise) delta wing with a chord length = 60 ft. and a maximum thickness ratio of 5% is used in the present investigation. The spanwise section of the wing is of diamond shape. The free stream Mach number is 2.0 and the wing altitude is 50,000 ft. The boom piece is made by taking a cross-section cut of the original Delta wing at x / L = 0.015625, and extending this cross section to a singular point at x = -0.10, y = 0, z = 0. The cross section is the same as that of the delta wing, which is a diamond shape in the spanwise direction. This cross-section decreases uniformly and linearly to the singular point at x = -0.10. This boom piece of 0.1 length of the wing chord is added at the wing vertex. The flow conditions considered here are: 2.24 deg. Angle of attack, 50000ft altitude and Mach number of 2.The delta wing flow without the boom piece has been solved using the CFL3D Euler equations near-field code and the full-potential equation far-field code. The interface between the near-field solver and the far-field solver is taken at h/L = 2.4. Next, the flow of the delta wing/boom piece configuration is solved using the same codes as those of the case above and for the same flow conditions. The density contours show the effect of the boom piece shock on the vertex shock of the delta wing. This interaction is clearly shown in Fig. 16 for the density contours in the plane of symmetry.

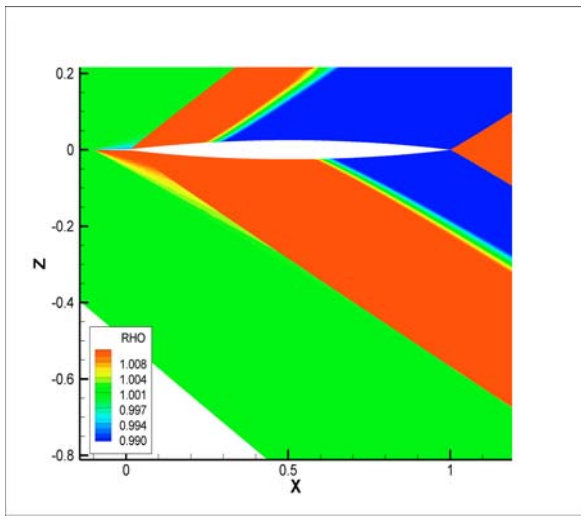

Fig. 16: Density contours for the delta wing/ boom piece configuration

Figure 16 shows a comparison of the overpressure versus the axial distance, X/L at h/L = 2.0 for the no-boom delta wing and the delta wing/boom piece configuration. . It is noticed that a reduction in leading (vertex) shock overpressure of 13.9 % is generated due to the boom piece, and a reduction in trailing shock overpressure of 37.2% is generated. The footprint of the delta wing/ boom piece configuration is reduced by 10.8%. These results (h/L = 2) are computed using the CFL3D

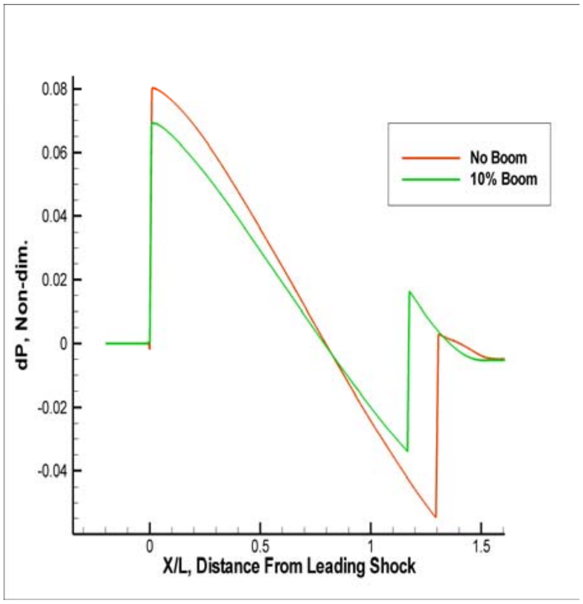

Fig. 17: Comparison of non-dimensional over pressures versus X/L at h / L = 2.0 below the delta wing; decrease in leading shock = 13.9%, decrease in trailing shock = 37.2%

The results show the remarkable effect of the boom piece on the reduction of the leading shock strength, the substantial reduction of the trailing shock strength, and the reduction of the foot-print width.

Next, we consider another case of sonic boom mitigation. Here, we consider the effect of the wing dihedral angle on the overpressure signal on the ground. The flow conditions are for M = 2 and altitude of 52,000ft. The wing is a delta wing with a maximum thickness ratio of 5%.

Figure 18, shows a comparison of the overpressure with the altitude for a delta wing with dihedral angles of 15^o and 20^o and a delta wing without dihedral angles (straight wing). Reductions of shock strength at the ground (sonic boom) ranged from 10 to 14 percent for wings with dihedral. Other techniques of sonic boom mitigation are being investigated. They include thickness, camber and nose angle variations. Sensitivity analysis and design optimization schemes are also being used.

5. Concluding Remarks

In this paper, sonic boom prediction, prediction of sonic boom focusing and sonic boom mitigation have been discussed and the state of the art has been presented. Additional work is still needed in the prediction area, where work is underway to convert the currently developed full-potential solver into a design tool without user interference. The Full-potential scheme can be coupled with the Ray linear scheme once the effect of nonlinearity ceases to affect the solution of the propagating wave at certain altitude. This approach would also expedite the currently parallel MPI full-potential solver. Work is progressing to come up with the optimum coupled schemes. The mitigation problem still needs substantial research work for investigating several techniques and hybrid techniques for mitigating the ground signature of the sonic boom. Sensitivity analysis and optimum designs will be substantially used to come up with these designs..

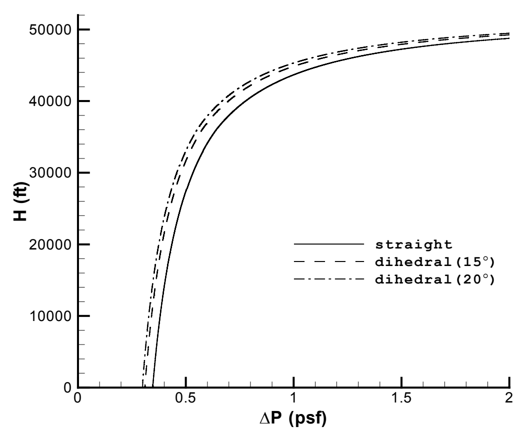

Figure 18. Variation of initial shock strength for straight and dihedral delta wings with altitude. 5% biconvex section, M = 2, H = 52,000ft. , c = 50ft., C_L = 0.077.

6. Acknowledgements

The recent part of this work (2004- present) has been developed under a grant support from the NASA Langley Research Center; Dr. Mujeeb Malik is the technical monitor. The early part of this work (2002-2004) was developed under two contracts from Eagle Aeronautics, Hampton, VA, Mr. Percy Bobbitt and NASA Langley Research Center, Mr. Peter Coen.

7. References

[1] Kandil, O. A. and Ozcer, I. A., "Sonic Boom Computations for Double-Cone Configuration Using CFL3D, FUN3D and Full-Potential Codes," AIAA 2006-0414, January 2006.

[2] Kandil, O. A., Ozcer, I. A., Zheng, X. and Bobbitt, P. J., "Comparison of Full-Potential Propagation-Code Computations with the F-5E "Shaped Sonic Boom Experiment" Program," AIAA 2005-0013, Reno, NV, January 2005.

[3] Ozcer, I. A., Sonic Boom Prediction using Euler/Full Potential Methodology, Master Thesis, Aerospace Engineering Department, Old Dominion University, Norfolk, VA, December 2005.

[4] Kandil, O. A.; Yang, Z.; Bobbitt, P. J., "Prediction of Sonic Boom Signature using Euler /Full Potential CFD with Grid Adaptation and Shock Fitting," AIAA CP 2002-2543, June 2002.

[5] Carlson, H. W., Mack, R. J. and Morris, O. A., "A wind-Tunnel Investigation of the effect of Body shape on Sonic-Boom Pressure Distribution," NASA TN D-3106, November 1965.

[6] Park, M. A., "Three-Dimensional Turbulent RANS Adjoint-Based Error Correction," AIAA 2003-3847, AIAA 16th Computational Fluid Dynamics Conference, Orlando, FL, June 2003.

[7] Anderson, W. K. and Bonhaus, D. L., "An Implicit Upwind Algorithm for Computing Turbulent Flows on Unstructured Grids," Computers and Fluids, Vol. 23, No. 1, 1994, pp. 1–22.

[8] Nielsen, E. J., Aerodynamic Design Sensitivities on an Unstructured Mesh Using the Navier-Stokes Equations and a Discrete Adjoint Formulation, Ph.D. thesis, Virginia Polytechnic Institute and State University, 1998.

[9] Guiraud, J.-P., "Acoustique geometrique, bruit balistique des avions supersoniques et focalization," J. Mecanique 4, 1965, pp 215-267.

[10] Hayes, W. D., "Similarity rules for nonlinear acoustic propagation through a caustic," Proceedings of the Sound Conference on Sonic Boom Research, NASA SP-180, 1968, pp 165-171.

[11] Hunter, J. K., "Caustics of Nonlinear Waves," Wave Motion 9, 1987, pp 429-443.

[12] Rosales, R. R. and Tabak, E. G., "Caustics of weak shock waves," Phys. Fluids 10, 1997, pp 206-222.

[13] Tabak, E. G. and Rosales, R. R., "Focusing of weak shock waves and the von Neumann paradox of oblique shock reflections," Phys. Fluids 6, 1994, pp 1874-1892.

[14] Augar, T. and Coulouvrat F., "Numerical Simulation of sonic Boom Focusing," AIAA J, Vol. 40, No. 9, September 2002, pp 1726- 1734.

[15] Marchiano, R. and Coulouvrat, F., "Numerical simulation of shock wave focusing at fold caustics with application to sonic boom," J. Acoust. Soc. Am. 114, No 4, October 2003, pp 1758-1771.

[16] Kandil, O. A. and Zheng, X., "Prediction of Superboom using Computational solution of Nonlinear Tricomi Equation," AIAA Paper 2005-6335, AIAA Atmospheric Flight Mechanics Conference, San Francisco, CA, August 2005.

[17] Kandil, O. A. and Zheng, X, "Computational solution of Nonlinear Tricomi Equation for sonic Boom Focusing and Applications," Paper Number 2005-43, International Sonic Boom Forum, Penn State University, PA, July 2005. Also in "Innovations in Nonlinear Acoustics", AIP Conference Proceedings, Melville, NY, 2006, Vol. 838, pp 607-610.

[18] Jones, L. B.: Lower Bounds for Sonic Bangs. J. Roy. Aeron. Soc. 65, 1-4 (1961).

[19] Jones, L. B.: Lower Bounds for Sonic Bang in the Far Field. Aeron. Quart. XVIII, Pt. 1, 1-21 (1967).

[20] Seebass, R.: Minimum Sonic Boom Shock Strengths and Overpressures. Nature 221, 651-653 (1969)

[21] Jones, L. B.: Lower Bounds for the Pressure Jump of the Bow Shock of a Supersonic Transport. The Acoustical Quarterly, Vol. XXI, Feb. 1970.

[22] George, A. R.; and Seebass, R.: Sonic Boom Minimization Including Both Front and Real Shocks. AIAA J. 9, 2091-2093 (1971).

[23] .Seebass, R.; and George, A. R.: Sonic-Boom Minimization. J. Acoust. Soc. Am., Vol. 51, No. 2 (pt. 3), Feb. 1972, pp. 686-694.

[24] Ferri, Antonio; and Schwartz, Ira R.: Sonic Boom Generation, Propagation, and Minimization. AIAA Paper No. 72-194, Jan. 1972.

[25] Carlson, Harry W., Barger, Raymond L.; and Mack, Robert J.: Application of Sonic-Boom Minimization Concepts in Supersonic Transport Design. NASA TN-D-7218, 1973.

[26] Darden, Christine, M.: Minimization of Sonic-Boom Parameters in Real and Isothermal Atmospheres. NASA TN D-7842, 1975.

[27] Darden, Christine M.: Sonic Boom Minimization With Nose-Bluntness Relaxation. NASA TP 1348, Jan. 1979.

[28] Mack, Robert J.; and Darden, Christine M.: Wind-Tunnel Investigation of the Validity of a Sonic-Boom-Minimization Concept. NASA TP 1421. October 1979.

[29] Hague, D. S.; and Jones, R. T.: Application of Multivariable Search Techniques to a Design of Low Sonic Boom Overpressure Body Shapes. NASA SP-255, pp. 307-323, Oct. 1970.

[30] Haglund, George T.: High Speed Civil Transport Design for Reduced Sonic Boom. Boeing Doc. No. D6-55430, NASA Cont. No. NAS1-18377, (1991)

[31] Mack, Robert J.; and Haglund, George T.: A Practical Low-Boom Overpressure Signature Based on Minimum Sonic Boom Theory. NASA C P-3173, Vol. II, pp. 15-19, Feb. 1992.

[32] Mack, Robert J.: Additional F-Functions Useful for Preliminary Design of Shaped Signature, Low-Boom, Supersonic-Cruise Aircraft. NASA CDCP-1001, pp. 1-12, Oct. 1994.

[33] Hunton, Lynn W.: Current Research in Sonic Boom. NASA SP-180, pp. 57-66, May 1968.

[34] Bobbitt, P., Kandil, O. A. and Yang, Z., "The Beneficial Effects of Wing Dihedral on Sonic Boom," AIAA paper 2003-3273-CP, Aeroacoustics Conf., Hilton Head, SC, 2003.